

MODELING OF METASHEETS EMBEDDED IN DIELECTRIC LAYERS

M. Y. Koledintseva^{1, *}, J. Huang², J. L. Drewniak¹,
R. E. DuBroff¹, and B. Archambeault³

¹Missouri University of Science and Technology, Rolla, MO 65409-0040, USA

²Nokia, San Diego, CA 92127, USA

³IBM, Research Triangle Park, NC, USA

Abstract—Metasheet structures together with bulk composite dielectric layers can be used for antenna radomes, absorbers, and band gap structures. Transmission (T) and reflection (Γ) coefficients for a plane wave incident at any angle upon a metasheet embedded in a dielectric layer are considered. These metasheets are either patch-type or an aperture-type, and they can be either single-layered or multi-layered. To calculate T and Γ for a patch-type metasheet, a concise unified matrix approach is derived using the Generalized Sheet Transition Conditions (GSTC). The Babinet duality principle is utilized to get T and Γ for single-layered aperture-type metasheets (as complementary to the patch-type ones) at an arbitrary angle of incidence. The \mathbf{T} -matrix approach is applied to calculate characteristics of multilayered metasheet structures containing a cascade of metasheets and dielectric slabs. In this paper, the minimum distance for neglecting higher-order evanescent mode interactions between the metasheets has been determined. Computed results based on the proposed analytical approach are compared with the full-wave numerical simulations. The analytical results are verified for satisfying the energy balance condition.

Received 9 July 2012, Accepted 11 September 2012, Scheduled 18 September 2012

* Corresponding author: Marina Y. Koledintseva (marinak@mst.edu).

1. INTRODUCTION

The development, research, and applications of metamaterials (MM), metafilms (MF), photonic bandgap (PBG) crystals, and artificial dielectric or magnetodielectric composite materials with desirable frequency responses are of an increased interest [1–5]. A metafilm, or a metasheet (MS), is the two-dimensional case of a metamaterial, and it can be either of a patch type (a dielectric film with identical metallic patches on it), or of an aperture type (conducting film with apertures, typically on a dielectric substrate). Thin planar metasheets find application over a wide range of frequencies from RF to the visual spectrum for designing antenna systems, filters, shielding enclosures, screens, and absorbers. Such structures have been studied, for example, for the development of frequency-selective surfaces (FSS) [6, 7], and for perforated film absorbers, such as CARAM (Circuit-Analog Radar Absorbing Materials) [8, 9]. FSS-based structures are used in antenna radomes [10], patch antennas [11], as well as controllable microwave absorbers [12].

Frequency characteristics of transmission (T) and reflection (Γ) coefficients of MS with simplest patterns have been analyzed using full-wave numerical methods, especially at arbitrary angles of electromagnetic incidence [13–15], as well as analytically (see, e.g., [16–20], and references therein). The generalized sheet transition condition (GSTC) for averaged *macroscopic* fields across a metafilm is proposed in [16]. GSTC relates field discontinuities to the electric and magnetic polarization densities of scatters on a metafilm. Based on the GSTC approach, the analytical formulas for T and Γ have been derived in [21], both for normal and oblique incidence. The GSTC approach is very attractive for designing metafilm shielding and filtering structures, since it substantially simplifies modeling and reduces computational resources, provided the polarizability of a desired pattern is determined in advance. A polarizability of interest may be retrieved comparatively easily either analytically or numerically, as is done in [22–26].

The formulation presented in [16] and [21] allows for treating polarizabilities only in the form of diagonal tensors, while the cross-coupling between electric and magnetic polarizabilities of metafilm elements is not taken into account. However, in many cases electric and magnetic cross-coupling cannot be neglected in principle, and the GSTC approach is not applicable to many pattern geometries. The examples of such pattern geometries are an edge-coupled split-ring resonator [27–29] and an Ω -particle used in chiral media [30]. Therefore one of the objectives of the present paper is to modify the GSTC for the case of cross-coupled electric and magnetic polarizabilities.

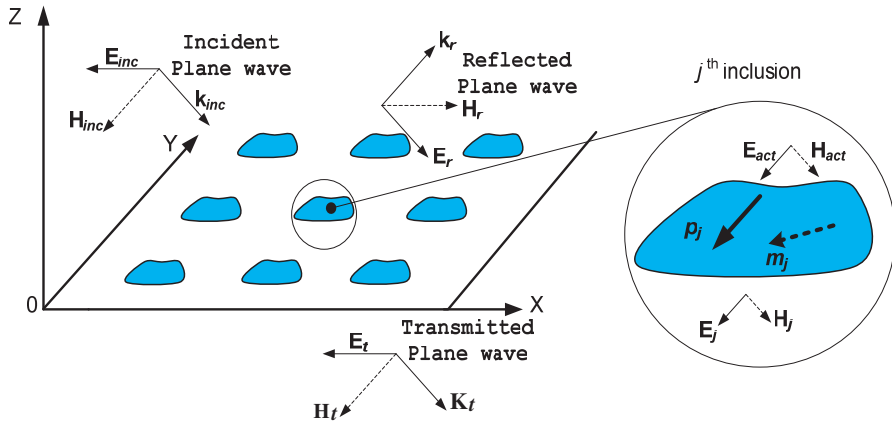


Figure 1. General geometry and main vectors describing interaction of a plane wave with a metasheet in cartesian coordinates.

Another objective is modeling multilayered metasheet structures, which provide more degrees of freedom in engineering material structures with desirable frequency responses. A problem is an interaction of individual metasheets through higher-order evanescent modes. However, when metasheets are placed far enough from each other, these evanescent modes can be neglected. Finding a distance between two neighboring metasheets, at which they can be considered as non-interacting, is an important issue.

It was shown that the GTSC analytical approach agrees well with numerical simulations for patch-type scatterers. However, analytical expressions in [16] and [21] for aperture structures should be modified to get better agreement. Herein, we generalize the formulation for both patch- and aperture-type metasheets, any shape of scatterers on a metasheet, an arbitrary number of layers, any frequency dispersion of a dielectric and/or magnetic media, in which these metasheets are embedded, and for all angles of a plane wave incidence.

2. GENERALIZED SHEET TRANSITION CONDITION (GSTC) FOR METASHEET

A general geometry of a metasheet is shown in Figure 1 in cartesian coordinates. For simplicity, assume that scatterers in the MS are small compared to a wavelength in the medium, and the MS is buried in a homogeneous host material with permittivity ϵ and permeability μ .

The electric and magnetic dipole moments associated with an

individual scatterer are expressed as

$$\begin{bmatrix} \vec{p} \\ \vec{m} \end{bmatrix} = \bar{a} \cdot \begin{bmatrix} \vec{E}^{\text{act}} \\ \vec{H}^{\text{act}} \end{bmatrix} = \begin{bmatrix} \bar{a}_{ee} & \bar{a}_{em} \\ \bar{a}_{me} & \bar{a}_{mm} \end{bmatrix} \cdot \begin{bmatrix} \vec{E}^{\text{act}} \\ \vec{H}^{\text{act}} \end{bmatrix}, \quad (1)$$

where $[\vec{E}^{\text{act}} \ \vec{H}^{\text{act}}]$ is the local acting electromagnetic field acting on the scatter; $\vec{p} = q\vec{l}$ and $\vec{m} = \pi \cdot r^2 I \cdot \hat{n}$ are the induced electric and magnetic dipoles, respectively; \bar{a}_{ee} , \bar{a}_{em} , \bar{a}_{me} , \bar{a}_{mm} are the 3×3 tensors denoting the electric (*ee*), magnetic (*mm*), and cross-coupling-electromagnetic (*em*) and magnetoelectric (*me*) polarizabilities from the *microscopic* point of view. The GSTC relates the discontinuity of the *macroscopic* field across the metasheet with *microscopic* polarizabilities of the scatters. The *macroscopic* field is defined as the superposition of an incident field and an induced secondary field from the metasheet, averaged in such a way that rapid variations of the field over a distance on the order of typical particle separations in the sheet are eliminated,

$$\begin{bmatrix} \vec{E} \\ \vec{H} \end{bmatrix} = \begin{bmatrix} \vec{E}^{\text{mac}} \\ \vec{H}^{\text{mac}} \end{bmatrix} = \begin{bmatrix} \vec{E}^{\text{inc}} \\ \vec{H}^{\text{inc}} \end{bmatrix} + \begin{bmatrix} \vec{E}^{\text{sheet}} \\ \vec{H}^{\text{sheet}} \end{bmatrix}. \quad (2)$$

In [16], the GSTC have been derived for the case without cross-coupling between electric and magnetic polarizations. Below, the GSTC are generalized for non-zero \bar{a}_{em} and \bar{a}_{me} .

The complete process can be divided into two steps: (1) the surface polarization and magnetization densities $[\vec{P}_s \ \vec{M}_s]$ are derived from the dipole polarizability tensor \bar{a} ; and (2) the discontinuity of the *macroscopic* field is expressed in terms of the *microscopic* polarizabilities by substituting the derived $[\vec{P}_s \ \vec{M}_s]$ into the boundary conditions

$$\begin{aligned} \hat{z} \times \vec{H} \Big|_{z=0^-}^{0^+} &= j\omega \vec{P}_{st} - \hat{z} \times \nabla_t \vec{M}_{sz}; \\ \vec{E} \Big|_{z=0^-}^{0^+} \times \hat{z} &= -j\omega \mu \vec{M}_{st} - \nabla_t \frac{\vec{P}_{sz}}{\epsilon} \times \hat{z}, \end{aligned} \quad (3)$$

where the boundary is located at $z = 0$. In (3), index “*t*” stands for transverse coordinates (x and y), and “*z*” corresponds to the z -components.

According to the Lorentz static field theory, only the dipole terms corresponding to the scatterers are considered for the induced field [31]. The induced field from the sheet is the superposition of the dipole fields of all the scatters in the infinite array. The acting field on the scatter under consideration (the j th scatterer) is the incident field, plus the field from all the neighboring dipoles (excluding the one under

consideration). The GSTC can be applied if two conditions are fulfilled. First, the scatters are densely packed, i.e., the distance between the scatterers is small compared with any large-scale dimension of the structure under consideration. This assures that the averaged field varies slowly enough, so that its discontinuity across the surface can be regarded as due to continuous surface distributions of \vec{P}_s and \vec{M}_s . Second, the distribution of the scatterers over the surface is sparse as measured in terms of the sizes of the scatterers themselves, i.e., interactions of the field from all the other scatterers on the scatterer under consideration can be replaced by a continuous distribution of \vec{P}_s and \vec{M}_s . This means that the j th scatterer can be replaced with an equivalent small disk of radius R centered at the position of the scatterer with uniformly distributed \vec{P}_s and \vec{M}_s , and the field from the neighboring scatterers acting on the j th scatter is modeled as a “punctured sheet” with the hole corresponding to the disk located at the j th scatterer (see Figure 1). The radius R is determined in [16] in the static limit $k \rightarrow 0$, assuming that the field of the punctured sheet is equal to the field caused by the dipole array constructed by all the discrete scatters, except the one to be studied. For example, $R \approx 0.6956D$ for a square array with the period D [32].

The acting field $[\vec{E}^{\text{act}} \quad \vec{H}^{\text{act}}]$ is then defined as the sum of the incident wave $[\vec{E}^{\text{inc}} \quad \vec{H}^{\text{inc}}]$ and the field from the entire sheet of the electric and magnetic polarization density $[\vec{E}^{\text{sheet}} \quad \vec{H}^{\text{sheet}}]$, excluding the contribution of a small disk under consideration $[\vec{E}^{\text{disk}} \quad \vec{H}^{\text{disk}}]$. Thus for the scatterer to be studied

$$\begin{aligned} \begin{bmatrix} \vec{E}^{\text{act}} \\ \vec{H}^{\text{act}} \end{bmatrix} &= \begin{bmatrix} \vec{E} - \vec{E}^{\text{disk}} \\ \vec{H} - \vec{H}^{\text{disk}} \end{bmatrix} \Big|_{z=0^+} = \begin{bmatrix} \vec{E} - \vec{E}^{\text{disk}} \\ \vec{H} - \vec{H}^{\text{disk}} \end{bmatrix} \Big|_{z=0^-} \\ &= \begin{bmatrix} \vec{E} \\ \vec{H} \end{bmatrix}_{av} - \begin{bmatrix} \vec{E}^{\text{disk}} \\ \vec{H}^{\text{disk}} \end{bmatrix}_{av}, \end{aligned} \tag{4}$$

where

$$\begin{aligned} \begin{bmatrix} \vec{E} \\ \vec{H} \end{bmatrix}_{av} &= \frac{1}{2} \left(\begin{bmatrix} \vec{E} \\ \vec{H} \end{bmatrix} \Big|_{z=0^+} + \begin{bmatrix} \vec{E} \\ \vec{H} \end{bmatrix} \Big|_{z=0^-} \right); \\ \begin{bmatrix} \vec{E}^{\text{disk}} \\ \vec{H}^{\text{disk}} \end{bmatrix}_{av} &= \frac{1}{2} \left(\begin{bmatrix} \vec{E}^{\text{disk}} \\ \vec{H}^{\text{disk}} \end{bmatrix} \Big|_{z=0^+} + \begin{bmatrix} \vec{E}^{\text{disk}} \\ \vec{H}^{\text{disk}} \end{bmatrix} \Big|_{z=0^-} \right), \end{aligned} \tag{5}$$

and \vec{E} and \vec{H} are the total fields.

The average field generated from the equivalent disk for the j th

scatter is [16]

$$\begin{bmatrix} \vec{E}^{\text{disk}} \\ \vec{H}^{\text{disk}} \end{bmatrix}_{av} = \bar{\bar{G}} \cdot \begin{bmatrix} \vec{P}_s \\ \vec{M}_s \end{bmatrix} \quad (6)$$

where $\bar{\bar{G}}$ is the diagonal matrix, derived in [16] assuming that near-field interactions are ignored for small kR with an error of $O\{(kR)^2\}$, where $k = \omega\sqrt{\varepsilon\mu}$,

$$\bar{\bar{G}} = \text{Diag} \left[-\frac{1}{4R\varepsilon} \quad -\frac{1}{4R\varepsilon} \quad \frac{1}{2R\varepsilon} \quad -\frac{1}{4R} \quad -\frac{1}{4R} \quad \frac{1}{2R} \right]. \quad (7)$$

Considering the relation between the electric and magnetic polarization densities and the electric and magnetic dipole moments given by

$$\begin{bmatrix} \vec{P}_s \\ \vec{M}_s \end{bmatrix} = N \left\langle \begin{bmatrix} \vec{p} \\ \vec{m} \end{bmatrix} \right\rangle, \quad (8)$$

where N is the number of scatters per unit area, and the symbol $\langle \rangle$ denotes averaging over the scatters in the vicinity of the points where P_s and M_s are defined. Substituting (1), (4), (6) in (8), a relation between polarization densities and *macroscopic* fields can be derived as

$$\begin{bmatrix} \vec{P}_s \\ \vec{M}_s \end{bmatrix} = N \left\langle \bar{\bar{\alpha}} \cdot \begin{bmatrix} \vec{E}^{\text{act}} \\ \vec{H}^{\text{act}} \end{bmatrix} \right\rangle = N \left\langle \bar{\bar{\alpha}} \cdot \left(\begin{bmatrix} \vec{E} \\ \vec{H} \end{bmatrix}_{av} - \bar{\bar{G}} \cdot \begin{bmatrix} \vec{P}_s \\ \vec{M}_s \end{bmatrix} \right) \right\rangle \quad (9)$$

For simplicity, assume that metasheet is a square array with the period D (center-to-center), so that

$$\begin{bmatrix} \vec{P}_s \\ \vec{M}_s \end{bmatrix} = \frac{1}{D^2} \begin{bmatrix} \vec{p} \\ \vec{m} \end{bmatrix} \quad (10)$$

Then, $[\vec{P}_s \quad \vec{M}_s]$ can be written through the *macroscopic* field as

$$\begin{bmatrix} \vec{P}_s \\ \vec{M}_s \end{bmatrix} = \left[D^2 \bar{\bar{\mathbf{I}}} + \bar{\bar{\alpha}} \cdot \bar{\bar{G}} \right]^{-1} \cdot \bar{\bar{\alpha}} \begin{bmatrix} \vec{E} \\ \vec{H} \end{bmatrix}_{av} = \bar{\bar{\alpha}}^{\text{mac}} \cdot \begin{bmatrix} \vec{E} \\ \vec{H} \end{bmatrix}_{av}, \quad (11)$$

where

$$\bar{\bar{\alpha}}^{\text{mac}} = \left[D^2 \bar{\bar{\mathbf{I}}} + \bar{\bar{\alpha}} \cdot \bar{\bar{G}} \right]^{-1} \cdot \bar{\bar{\alpha}} = \begin{bmatrix} \bar{\bar{\alpha}}_{EE} & \bar{\bar{\alpha}}_{EM} \\ \bar{\bar{\alpha}}_{ME} & \bar{\bar{\alpha}}_{MM} \end{bmatrix} \quad (12)$$

is the macroscopic polarizability tensor relating the polarization density to the *macroscopic* field, and is a function of the periodicity of the array and the polarizabilities of the inclusions. $\bar{\bar{\mathbf{I}}}$ is the unity tensor.

Substituting (11) in (3) to replace the surface polarization and magnetization with the *macroscopic* field terms, the GSTC that includes *macroscopic* polarizabilities [33, 34] is

$$\begin{aligned} \hat{z} \times \vec{H} \Big|_{z=0^-}^{0^+} &= j\omega [\bar{\alpha}_{EE,t} \quad \bar{\alpha}_{EM,t}] \cdot \left[\begin{array}{c} \vec{E} \\ \vec{H} \end{array} \right]_{av} \\ &\quad - \hat{z} \times \nabla_t \left([\bar{\alpha}_{ME,z} \quad \bar{\alpha}_{MM,z}] \cdot \left[\begin{array}{c} \vec{E} \\ \vec{H} \end{array} \right]_{av} \right); \\ \vec{E} \Big|_{z=0^-}^{0^+} \times \hat{z} &= -j\omega\mu [\bar{\alpha}_{ME,t} \quad \bar{\alpha}_{MM,t}] \cdot \left[\begin{array}{c} \vec{E} \\ \vec{H} \end{array} \right]_{av} \\ &\quad - \frac{1}{\varepsilon} \nabla_t \left([\bar{\alpha}_{EE,z} \quad \bar{\alpha}_{EM,z}] \cdot \left[\begin{array}{c} \vec{E} \\ \vec{H} \end{array} \right]_{av} \right) \times \hat{z}. \end{aligned} \quad (13)$$

The coordinate system is as in Figure 1. The left-hand sides of (13) are the field discontinuities, while the right-hand side is the average field across the sheet. The field relation across the sheet is solely governed by the array period and the geometry parameters of the scatterer. Further, using (13), the field discontinuity across the metasheet will be expressed through the incident, reflected and transmitted components, and T and Γ will be calculated. The reflection and transmission coefficients also depend on the array period and geometry of scatterers.

3. T AND Γ FOR A SINGLE-LAYERED METASHEET

A case of an arbitrary angle of incidence θ of a plane wave upon a single metasheet is considered herein. The transmission T and reflection Γ coefficients are derived for both patch-type and aperture-type metasheets. For a patch-type metasheet, a system of two linear

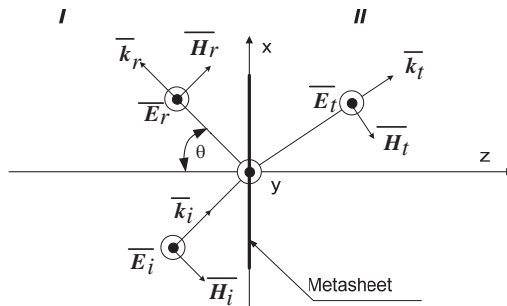


Figure 2. TE plane wave incident on a metasheet.

equations for T and Γ is solved, and for an aperture-type metasheet, the Babinet's duality principle [35, 36] is used to map T and Γ from the complementary patch-type problem. It is easy to verify that the formulas obtained below for the GSTC, T and Γ converge to those obtained in [16] and [21]. However, this is valid for the case, when the cross-coupling terms in the polarizability tensor tend to zero. It should be mentioned that the similar approach can be used in a straightforward manner for the general case of non-zero cross-coupling (non-diagonal polarizability tensor), and this is the subject for the future paper.

3.1. TE Plane Wave Incident on a Patch-type Metasheet

Incident, reflected, and transmitted electric and magnetic fields are shown in Figure 2 for a metasheet located in the plane $z = 0$. The expressions for the corresponding fields are as in [37],

$$\begin{aligned}
 \vec{E}_i &= \hat{y}E_0e^{-j\bar{k}_i\cdot\bar{r}}; & \vec{E}_r &= \hat{y}\Gamma_{TE}E_0e^{-j\bar{k}_r\cdot\bar{r}}; & \vec{E}_t &= \hat{y}T_{TE}E_0e^{-j\bar{k}_t\cdot\bar{r}}; \\
 \bar{H}_i &= \frac{E_0}{\eta}(-\hat{x}\cos\theta + \hat{z}\sin\theta)e^{-j\bar{k}_i\cdot\bar{r}}; \\
 \bar{H}_r &= \frac{E_0}{\eta}\Gamma_{TE}(\hat{x}\cos\theta + \hat{z}\sin\theta)e^{-j\bar{k}_r\cdot\bar{r}}; \\
 \bar{H}_t &= \frac{E_0}{\eta}T_{TE}(-\hat{x}\cos\theta + \hat{z}\sin\theta)e^{-j\bar{k}_t\cdot\bar{r}}.
 \end{aligned} \tag{14}$$

In (14), $\bar{r} = \hat{x}x + \hat{y}y + \hat{z}z$ is the radius-vector of the point of observation; $\eta = \sqrt{\frac{\mu}{\varepsilon}}$ is the characteristic impedance of the host medium, and the incident, transmitted, and reflected wave vectors are

$$\begin{aligned}
 \bar{k}_i &= \bar{k}_t = (\hat{x}\sin\theta + \hat{z}\cos\theta)k; \\
 \bar{k}_r &= (\hat{x}\sin\theta - \hat{z}\cos\theta)k.
 \end{aligned} \tag{15}$$

T_{TE} and Γ_{TE} are the transmission and reflection coefficients for an incident TE plane wave. Defining the forward vector \bar{C}_{TE}^+ and the backward vector \bar{C}_{TE}^- ,

$$\begin{aligned}
 \bar{C}_{TE}^+ &= \left[0 \ 1 \ 0 \ -\frac{\cos\theta}{\eta} \ 0 \ \frac{\sin\theta}{\eta} \right]^T; \\
 \bar{C}_{TE}^- &= \left[0 \ 1 \ 0 \ \frac{\cos\theta}{\eta} \ 0 \ \frac{\sin\theta}{\eta} \right]^T,
 \end{aligned} \tag{16}$$

one can write the total field in regions 1 and 2 as

$$\begin{aligned} \begin{bmatrix} \vec{E} \\ \vec{H} \end{bmatrix}_{z<0} &= \begin{bmatrix} \vec{E}_i \\ \vec{H}_i \end{bmatrix} + \begin{bmatrix} \vec{E}_r \\ \vec{H}_r \end{bmatrix} = E_0 (\bar{C}_{TE}^+ + \Gamma_{TE} \bar{C}_{TE}^-); \\ \begin{bmatrix} \vec{E} \\ \vec{H} \end{bmatrix}_{z>0} &= \begin{bmatrix} \vec{E}_t \\ \vec{H}_t \end{bmatrix} = E_0 T_{TE} \bar{C}_{TE}^+. \end{aligned} \quad (17)$$

The average field is

$$\begin{bmatrix} \vec{E} \\ \vec{H} \end{bmatrix}_{av} = E_0 \left[\frac{\bar{C}_{TE}^+ + \Gamma_{TE} \bar{C}_{TE}^- + T_{TE} \bar{C}_{TE}^+}{2} \right]_{z=0}, \quad (18)$$

and the field jump at the boundary is

$$\begin{bmatrix} \vec{E} \\ \vec{H} \end{bmatrix} \Big|_{z=0^-}^{z=0^+} = E_0 [T_{TE} \bar{C}_{TE}^+ - (\bar{C}_{TE}^+ + \Gamma_{TE} \bar{C}_{TE}^-)]_{z=0}. \quad (19)$$

For the TE wave $\frac{\partial}{\partial x} = -jk \sin \theta$ and $\frac{\partial}{\partial y} = 0$, and the GSTC (13) can be written as

$$\begin{aligned} & [0 \ 0 \ 0 \ 1 \ 0 \ 0] \cdot (\mathbf{C}_{TE}^+ T_{TE} - \mathbf{C}_{TE}^- \Gamma_{TE} - \mathbf{C}_{TE}^+) \\ &= [0 \ j\omega \ 0 \ 0 \ 0 \ jk \sin \theta] \cdot [\bar{\alpha}^{\text{mac}}] \cdot \frac{C_{TE}^+ T_{TE} + C_{TE}^- \Gamma_{TE} + C_{TE}^+}{2}; \end{aligned} \quad (20a)$$

$$\begin{aligned} & [0 \ 1 \ 0 \ 0 \ 0 \ 0] \cdot (\mathbf{C}_{TE}^+ T_{TE} - \mathbf{C}_{TE}^- \Gamma_{TE} - \mathbf{C}_{TE}^+) \\ &= [0 \ 0 \ 0 \ j\omega \mu \ 0 \ 0] \cdot [\bar{\alpha}^{\text{mac}}] \cdot \frac{C_{TE}^+ T_{TE} + C_{TE}^- \Gamma_{TE} + C_{TE}^+}{2}. \end{aligned} \quad (20b)$$

In a compact matrix form, the system of linear equations with respect to the unknowns T_{TE} and Γ_{TE} is then

$$\begin{bmatrix} A_{1,TE} & A_{2,TE} \\ 1 & -1 \end{bmatrix} \cdot \begin{bmatrix} T_{TE} \\ \Gamma_{TE} \end{bmatrix} = \begin{bmatrix} A_{3,TE} \\ 1 \end{bmatrix}, \quad (21)$$

where

$$\begin{aligned} A_{1,TE} &= \left([0 \ 0 \ 1 \ 0 \ 0] - \left[0 \ \frac{jk}{2\varepsilon} \ 0 \ 0 \ 0 \ \frac{jk \sin \theta}{2} \right] \cdot [\bar{\alpha}^{\text{mac}}] \right) \cdot \bar{C}_{TE}^+; \\ A_{2,TE} &= - \left([0 \ 0 \ 0 \ 1 \ 0 \ 0] + \left[0 \ \frac{jk}{2\varepsilon} \ 0 \ 0 \ 0 \ \frac{jk \sin \theta}{2} \right] \cdot [\bar{\alpha}^{\text{mac}}] \right) \cdot \bar{C}_{TE}^-; \\ A_{3,TE} &= \left([0 \ 0 \ 0 \ 1 \ 0 \ 0] + \left[0 \ \frac{jk}{2\varepsilon} \ 0 \ 0 \ 0 \ \frac{jk \sin \theta}{2} \right] \cdot [\bar{\alpha}^{\text{mac}}] \right) \cdot \bar{C}_{TE}^+. \end{aligned} \quad (22)$$

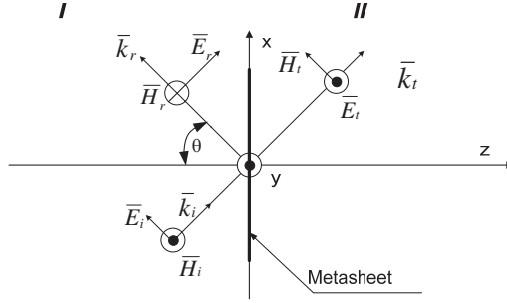


Figure 3. *TM* plane wave incident on a metasheet.

3.2. *TM* Incident Plane Wave on a Metasheet

The *TM* plane wave incident on a metasheet is shown in Figure 3.

Using the same expression for the fields as in [37], and defining the forward and backward vectors as

$$\begin{aligned} \bar{C}_{TM}^+ &= \left[\cos \theta \quad 0 \quad -\sin \theta \quad 0 \quad \frac{1}{\eta} \quad 0 \right]^T; \\ \bar{C}_{TM}^- &= \left[\cos \theta \quad 0 \quad \sin \theta \quad 0 \quad -\frac{1}{\eta} \quad 0 \right]^T, \end{aligned} \quad (23)$$

respectively, a system of linear equations analogous to (21) can be written as

$$\begin{bmatrix} A_{1,TM} & A_{2,TM} \\ 1 & -1 \end{bmatrix} \cdot \begin{bmatrix} T_{TM} \\ \Gamma_{TM} \end{bmatrix} = \begin{bmatrix} A_{3,TM} \\ 1 \end{bmatrix}, \quad (24)$$

where

$$\begin{aligned} A_{1,TM} &= \left([0 \ 0 \ 0 \ 0 \ 1 \ 0] + \left[\frac{j\omega}{2} \ 0 \ 0 \ 0 \ 0 \ 0 \right] \cdot [\bar{\alpha}^{\text{mac}}] \right) \cdot \bar{C}_{TM}^+; \\ A_{2,TM} &= \left(-[0 \ 0 \ 0 \ 0 \ 1 \ 0] + \left[\frac{j\omega}{2} \ 0 \ 0 \ 0 \ 0 \ 0 \right] \cdot [\bar{\alpha}^{\text{mac}}] \right) \cdot \bar{C}_{TM}^-; \\ A_{3,TM} &= \left([0 \ 0 \ 0 \ 0 \ 1 \ 0] - \left[\frac{j\omega}{2} \ 0 \ 0 \ 0 \ 0 \ 0 \right] \cdot [\bar{\alpha}^{\text{mac}}] \right) \cdot \bar{C}_{TM}^+. \end{aligned} \quad (25)$$

3.3. Transmission and Reflection Coefficients for an Aperture-type Metasheet

The reflection and transmission coefficients T and Γ for aperture-type metasheets cannot be calculated by directly applying the corresponding polarizabilities to the GSTC. For example, if there is a circular aperture array with a normally incident plane wave, the

only non-zero components of the polarizability tensor are α_{EE}^{zz} , α_{MM}^{xx} and α_{MM}^{yy} . Then the expressions that coincide with (20), (24) in [21] for $\theta = 0$ are

$$\begin{aligned} T_{TE} &= \frac{1}{1 - j \frac{k\alpha_{MM}^{xx}}{2}}; & \Gamma_{TE} &= \frac{-j \frac{k\alpha_{MM}^{xx}}{2}}{1 - j \frac{k\alpha_{MM}^{xx}}{2}}; \\ T_{TM} &= \frac{1}{1 - j \frac{k\alpha_{MM}^{yy}}{2}}; & \Gamma_{TM} &= \frac{-j \frac{k\alpha_{MM}^{yy}}{2}}{1 - j \frac{k\alpha_{MM}^{yy}}{2}}. \end{aligned} \quad (26)$$

Then T corresponds to a low-pass frequency response, which conflicts with the expected high-pass characteristics [18], as well as with the full-wave simulations. As is indicated in [16], further treatment is needed to generalize the GSTC for the aperture-type case.

The obstacles in applying the GSTC formulation directly to aperture-type metasheets can be overcome by solving the problem formulated for the corresponding patch-type complementary structure. Then, using the Babinet principle [18, 35], it is easy to map the results into Γ and T of the aperture-type metasheet. The relations between Γ and T of complementary arrays under normal incidence are [18]

$$T_{\text{patch}} = -\Gamma_{\text{aperture}} \quad \text{and} \quad \Gamma_{\text{patch}} = -T_{\text{aperture}}. \quad (27)$$

Below, this complementary principle is generalized for an arbitrary angle of incidence. In Figure 4(a), the surface $\sum a$ denotes an aperture, and the surface $\sum \tilde{a}$ denotes a perfect electric conductor (PEC). In the complementary structure in Figure 4(b), $\sum a$ is a PEC, and $\sum \tilde{a}$ is an aperture.

If $[T_{TE} \ \Gamma_{TE}]$ corresponds to a metasheet, then $[\tilde{T}_{TM} \ \tilde{\Gamma}_{TM}]$ corresponds to the complementary metasheet, where TE plane wave polarization is complementary to the TM plane wave polarization. Then the following relations between the reflection and transmission coefficients for the aperture and the patch problems are

$$T_{TE} = -\tilde{\Gamma}_{TM} \quad \text{and} \quad \Gamma_{TE} = -\tilde{T}_{TM}. \quad (28)$$

The detailed derivation of these relations is given in Appendix A. Therefore, Γ and T of an aperture-type metasheet for both TE and TM polarizations can be mapped from the results of the complementary metasheet. It is important to note that for considering aperture-type and patch-type metasheets as complementary, they must be embedded in the same media.

4. MULTILAYERED METASHEETS

Metasheets may be stacked together with the dielectric or composite slabs in some practical applications to get the desirable frequency

response for Γ and T . The \mathbf{T} -matrix (transfer-matrix) approach is convenient to get Γ and T expressions for a plane wave incident at an arbitrary angle upon the multilayered metasheets (cascade of metasheet and dielectric slabs). The \mathbf{T} -matrix cascading is helpful not only for the reflected and transmitted wave analysis, but also for the process of synthesis of a structure with the required frequency characteristics. For simplicity, assume that a metasheet is buried inside a homogeneous host material.

4.1. T-Matrix Approach

The \mathbf{T} -matrix, illustrated by Figure 5, is a type of a chain matrix convenient for modeling the wave-transmission system as a two-port network that relates the forward and backward waves at the input and output ports [38].

$$\begin{bmatrix} a_1 \\ b_1 \end{bmatrix} = \begin{bmatrix} t_{11} & t_{12} \\ t_{21} & t_{22} \end{bmatrix} \cdot \begin{bmatrix} b_2 \\ a_2 \end{bmatrix}, \quad (29)$$

where a_1 and b_2 are the forward waves, and b_1 and a_2 are the backward waves.

The reflection and transmission coefficients Γ and T can be derived using the definitions

$$\Gamma = \Gamma_{11} = \left. \frac{b_1}{a_1} \right|_{a_2=0} \quad \text{and} \quad T = T_{21} = \left. \frac{b_2}{a_1} \right|_{a_2=0}. \quad (30)$$

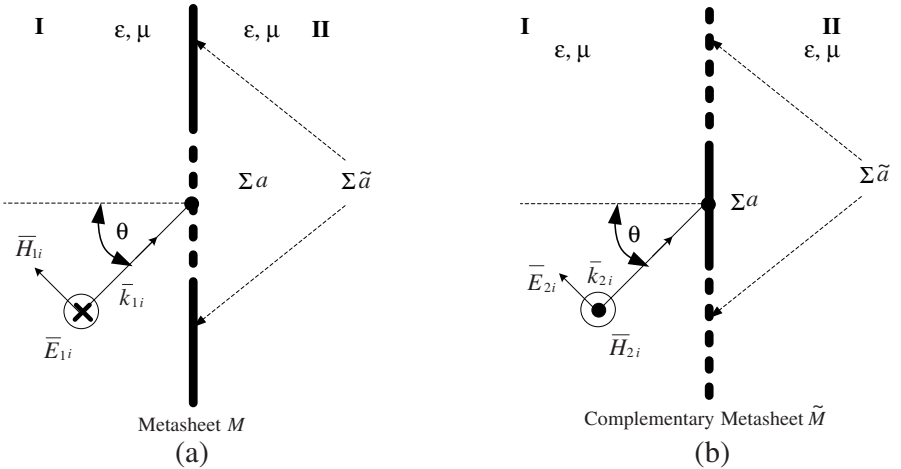


Figure 4. Wave incidence upon a PEC screen with an (a) aperture, and the (b) complementary problem.

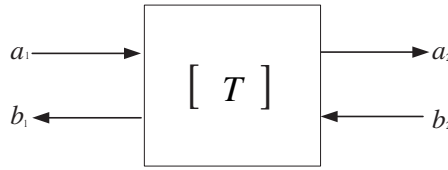


Figure 5. Definition of incoming and outgoing waves in the **T**-matrix.

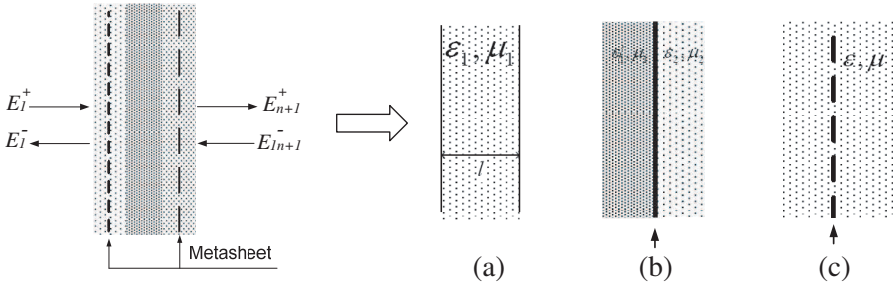


Figure 6. Decomposition of multilayered metasheet. (a) Medium slab. (b) Medium interface. (c) Metasheet.

The **T**-matrix of N cascaded 2-port networks T_1, T_2, \dots, T_N is the product of the corresponding **T**-matrices,

$$T_{\text{tot}} = \begin{bmatrix} t_{11} & t_{12} \\ t_{21} & t_{22} \end{bmatrix} = T_1 \cdot T_2 \dots T_N. \tag{31}$$

Then, Γ and T for the multilayered metasheet can be easily derived with (30).

4.2. T-Matrix for a Multilayered Metasheet

Any individual metasheet embedded in a dielectric can be decomposed into three basic elements: (a) a host medium slab, (b) a medium interface, and, (c) a metasheet inside the homogeneous host medium, as shown in Figure 6. The overall **T**-matrix is a product of the partial **T**-matrices of these basic elements, and then Γ and T of the whole structure can be easily obtained.

According to [31], the **T**-matrix for a slab of a homogeneous medium of thickness l is defined as

$$T_S = \begin{bmatrix} e^{jkl \cos \theta} & 0 \\ 0 & e^{-jkl \cos \theta} \end{bmatrix}. \tag{32}$$

The **T**-matrix for a medium interface is

$$T_I = \frac{1}{\tau_{T1}} \begin{bmatrix} 1 & \rho_{T1} \\ \rho_{T1} & 1 \end{bmatrix}, \tag{33}$$

where

$$\begin{aligned} \tau_{T1} &= \frac{\eta_{T2} - \eta_{T1}}{\eta_{T2} + \eta_{T1}}, & \rho_{T1} &= \frac{2\eta_{T2}}{\eta_{T2} + \eta_{T1}}, \\ \text{and } \eta_{T1,2} &= \begin{cases} \frac{1}{\cos \theta} \sqrt{\frac{\mu_{1,2}}{\varepsilon_{1,2}}} & \text{for } TE \\ \sqrt{\frac{\mu_{1,2}}{\varepsilon_{1,2}}} \cos \theta & \text{for } TM \end{cases}. \end{aligned} \quad (34)$$

are the corresponding transmission and reflection coefficients, and the characteristic impedance.

The \mathbf{T} -matrix for a metasheet buried in the homogeneous host material can be obtained through the S -parameter matrix for a metasheet. Suppose that the transmission and reflection coefficients for an individual metasheet $\Gamma_{TE, TM}$ and $T_{TE, TM}$ are known, then the corresponding S -parameter matrix is related to the reflection and transmission coefficients as (if the second port is matched),

$$s_{M_{TE, TM}} = \begin{bmatrix} \Gamma_{TE, TM} & T_{TE, TM} \\ T_{TE, TM} & \Gamma_{TE, TM} \end{bmatrix}, \quad (35)$$

and the corresponding \mathbf{T} -matrix is easily derived from (35),

$$T_{M_{TE, TM}} = \frac{1}{T_{TE, TM}} \begin{bmatrix} 1 & -\Gamma_{TE, TM} \\ \Gamma_{TE, TM} & T_{TE, TM}^2 - \Gamma_{TE, TM}^2 \end{bmatrix}. \quad (36)$$

4.3. Distance Requirement Between the Neighboring Metasheets

An incident wave scattering from an array of patches or apertures results in the excitation of the evanescent modes in addition to the propagating wave, when the array period is smaller than the wavelength [18]. The distance d between metasheets should be kept large enough to assure that the evanescent waves decay sufficiently and do not couple to the adjacent sheet. Otherwise, the expressions for Γ and T derived for propagating waves, will be not valid. The requirement to the distance d between the neighboring metasheets can be obtained assuming that the amplitudes of all the evanescent waves, normalized to the propagating wave amplitude, are smaller than some required value δ .

The total scattered field can be expressed in terms of the Floquet

space harmonics as a double Fourier expansion [18],

$$\vec{E}(\vec{r}) = \begin{cases} \hat{u}T e^{-jkz} + \hat{u} \sum_p \sum_q T_{pq} Q_{pq}(x, y) e^{-j\gamma_{pq}z} & z > 0 \\ \hat{u}\Gamma e^{jkz} + \hat{u} \sum_p \sum_q \Gamma_{pq} Q_{pq}(x, y) e^{j\gamma_{pq}z} & z < 0 \end{cases}, \quad (37)$$

where T_{pq} and Γ_{pq} are transmission and reflection coefficients of the high-order modes with indices $p = q = 0, \pm 1, \pm 2, \dots$, except for $p = q = 0$, and the propagation constants are $\gamma_{pq} = \sqrt{k^2 - (\frac{2\pi}{D})^2 (p^2 + q^2)}$. In (37), the transverse exponential factor is

$$Q_{pq} = \exp \left[-j \frac{2\pi}{D} (px + qy) \right]. \quad (38)$$

The higher-order modes become evanescent, when $D < \lambda$. This means that d should be large enough to satisfy the inequalities

$$\left| T_{pq} Q_{pq}(x, y) e^{-j\gamma_{pq}d} \right| < \delta T \quad \text{and} \quad \left| \Gamma_{pq} Q_{pq}(x, y) e^{j\gamma_{pq}d} \right| < \delta \Gamma \quad (39)$$

The evanescent mode with $p = 1, q = 0$ (or $p = 0, q = 1$) is studied here, since it has the largest amplitude for a parallel-plane geometry. To get an accurate value of d_{\min} , a numerical evaluation for T_{pq} and Γ_{pq} can be used. However, herein, the first-order accuracy estimation based on a very coarse presumption of $T_{pq}/T = 1$ and $\Gamma_{pq}/\Gamma = 1$ can be obtained

$$d > \frac{-\ln \delta}{2\pi \sqrt{(\frac{1}{D})^2 + (\frac{1}{\lambda})^2}}. \quad (40)$$

Numerous simulations indicate that the accuracy of the analytical approach used herein for a multilayered metasheet is quite satisfactory for $\delta < 0.1$.

5. VERIFICATION

5.1. Verification of the Analytical Formulas with Energy Conservation for a Lossless Metasheet

A polarizability tensor of any lossless patch-type metasheet, containing PEC scatterers, has the following properties:

(a) Reciprocity is fulfilled [18]:

$$\bar{\bar{\alpha}}_{ee} = \bar{\bar{\alpha}}_{ee}^T, \quad \bar{\bar{\alpha}}_{mm} = \bar{\bar{\alpha}}_{mm}^T, \quad \bar{\bar{\alpha}}_{em} = -\mu \bar{\bar{\alpha}}_{me}^T. \quad (41)$$

(b) There is only the tangential current induced, so there is no electric dipole in the normal direction, and no magnetic dipole in

the tangential direction. At the same time, considering (41), the polarizability tensor has the following format:

$$\begin{bmatrix} \otimes & \otimes & 0 & 0 & 0 & \otimes \\ \otimes & \otimes & 0 & 0 & 0 & \otimes \\ 0 & 0 & 0 & 0 & 0 & 0 \\ 0 & 0 & 0 & 0 & 0 & 0 \\ 0 & 0 & 0 & 0 & 0 & 0 \\ \otimes & \otimes & 0 & 0 & 0 & \otimes \end{bmatrix}. \quad (42)$$

where \otimes denotes non-zero elements.

(c) $\bar{\alpha}_{ee}$, $\bar{\alpha}_{mm}$ are the real matrices, while $\bar{\alpha}_{em}$ and $\bar{\alpha}_{me}$ are the imaginary matrices.

(d) The macroscopic polarizability $\bar{\alpha}^{\text{mac}}$ derived from (12) also has the properties (a)–(c). Specifically, the reciprocity property can be expressed as

$$\bar{\alpha}_{EE} = \bar{\alpha}_{EE}^T, \quad \bar{\alpha}_{MM} = \bar{\alpha}_{MM}^T, \quad \bar{\alpha}_{EM} = -\mu \bar{\alpha}_{ME}^T. \quad (43)$$

The proof for (d) is cumbersome, but it can be done by processing (12) with a symbolic software tool, e.g., Mathematica.

Based on these properties, one can get that for any metasheet made of a PEC, the energy conservation relation always holds for TE and TM modes and any angle of incidence, i.e.,

$$|T|^2 + |\Gamma|^2 = 1, \quad TE \text{ or } TM. \quad (44)$$

This is detailed in Appendix B.

5.2. Verification for \mathbf{T} and $\mathbf{\Gamma}$ of a Single-layered Metasheet

5.2.1. Disc Array

The geometry of a disc array is shown in Figure 7. The cell period is $D = 12$ mm, disc radius is $a = 5$ mm, and the host medium is

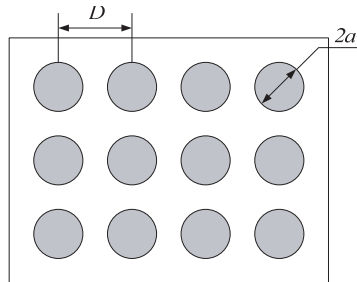


Figure 7. Geometry of the disc array.

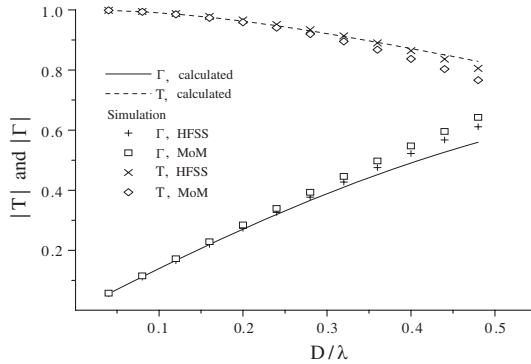


Figure 8. T and Γ at normal incidence upon a disk array.

vacuum. The calculation based on the proposed analytical formulation and the simulation results obtained using the commercial software ANSYS HFSS and Ansoft Designer (MoM) are shown in Figure 8.

The results of computations agree well in a low-frequency range (or $D/\lambda < 0.4$). However, with the increase of frequency (or $D/\lambda > 0.4$), the discrepancy increases. This is because only the dipole moment is considered in the quasi-static analytical solution. More accurate result is expected, when the dynamic interaction and higher order polarizations are taken into account [39, 40].

5.2.2. Edge-coupled Split-ring Resonator with Cross-coupling

Edge-coupled split-ring resonator (EC-SRR) shown in Figure 9 is a typical scatter that has electric and magnetic cross-coupling. Its polarizability components are

$$\begin{aligned}
 p_x &= \alpha_{xx}^{ee} E_x^{\text{act}}; & p_y &= (\alpha_{yy}^{ee} + \alpha_{yy}'^{ee}) E_y^{\text{act}} + j\alpha_{yz}^{em} B_z^{\text{act}}; \\
 m_z &= \alpha_{zz}^{mm} B_z^{\text{act}} - j\alpha_{yz}^{em} E_y^{\text{act}}
 \end{aligned}
 \tag{45}$$

The components of the tensor $\bar{\bar{\alpha}}$ in (44) can be calculated using the formulas in [27]. The parameters of the modeled EC-SRR are the following: the cell period is $D = 8$ mm, the external radius is $r_{\text{ext}} = 2.6$ mm, the trace width is $c = 0.5$ mm, the gap width is $d = 0.2$ mm, $\epsilon_r = 1$, and thickness of the dielectric slab is $t = 0.49$ mm. As is seen from Figure 10, in the low-frequency range the agreement is better than at higher frequencies. The higher accuracy at higher frequencies may be achieved with more accurate modeling of the polarizabilities of the EC-SRR.

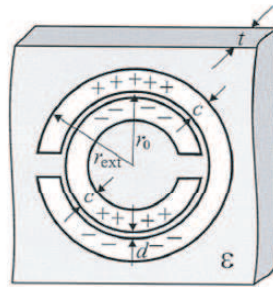


Figure 9. Geometry of the EC-SRR [27].

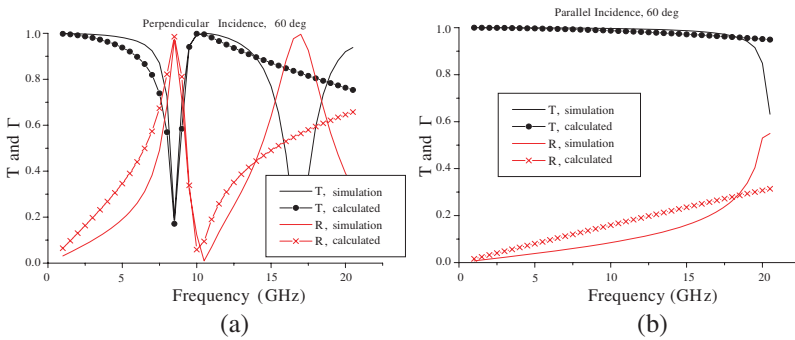


Figure 10. T and Γ for the EC-SRR at the oblique incidence: (a) TE incidence with $\theta = 60^\circ$; (b) TM incidence with $\theta = 60^\circ$.

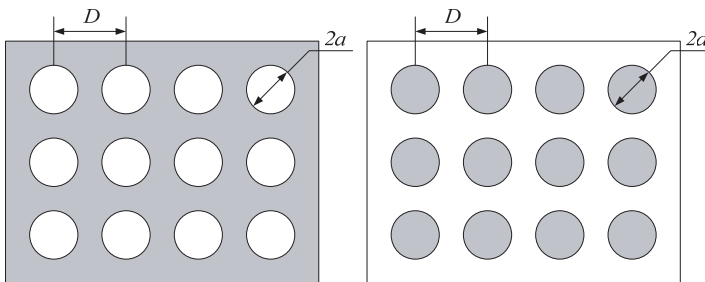


Figure 11. Geometry of aperture array and its complementary structure.

5.2.3. Aperture Structure: Utilization of the Babinet's Principle

The geometry of an aperture array and its complementary structure are shown in Figure 11. The cell period is $D = 12$ mm, the radius is $a = 5$ mm, and $\varepsilon_r = 1$. Figure 12 shows the results mapped from the complementary disk array and those simulated using HFSS. Their good agreement justifies the feasibility of the obtained analytical solution for

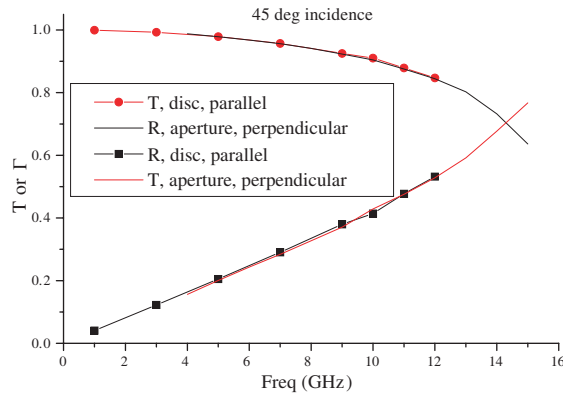


Figure 12. T and Γ of an aperture array and its complementary structure.

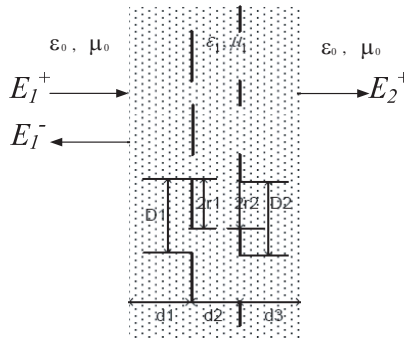


Figure 13. Geometry of a multilayered metasheet.

aperture-type metasheets.

5.3. Multilayered Metasheet Structure

5.3.1. Lossless Medium

The geometry of the two-layered structure with a disc array metasheet and an aperture array metasheet is shown in Figure 13. The array periods of the metasheets are $D1 = D2 = 12\text{ mm}$, their radii are $r1 = r2 = 5\text{ mm}$, and the distance between the metasheets is $d = 6\text{ mm}$. Analytical and numerical simulation results almost coincide in the considered frequency range up to 15 GHz.

5.3.2. Requirement for a Separation Distance between Metasheets

According to the simulations, when d is so small that the corresponding parameter $\delta > 10\%$ in (40), the accuracy of calculating T and Γ degrades greatly. Thus, for the same geometry as in Figure 13, when $d = 3$ mm and $\delta = 28\%$, there is an apparent frequency shift observed, as shown in Figure 14. At the same time, Figure 15 shows that when $d = 6$ mm and δ reduces to 8%, there is a good agreement between the analytical computations and numerical simulations.

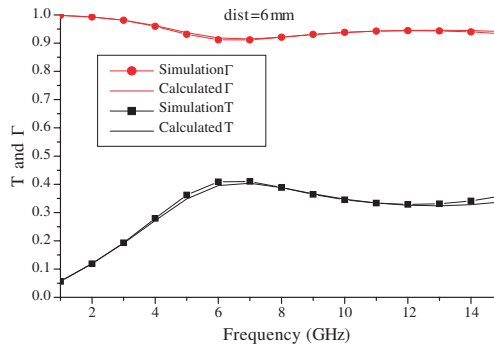


Figure 14. Comparison of analytically calculated and numerically simulated results for transmission (T) and reflection (Γ) coefficients for a multilayered metasheet, when the distance between the metasheets is comparatively large ($d = 6$ mm).

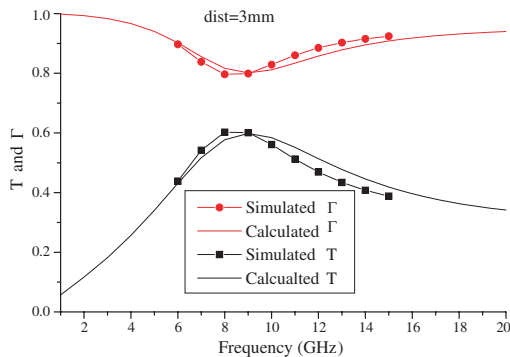


Figure 15. Comparison of analytically calculated and numerically simulated results for transmission (T) and reflection (Γ) coefficients for a multilayered metasheet, when the distance between the metasheets is comparatively small ($d = 3$ mm).

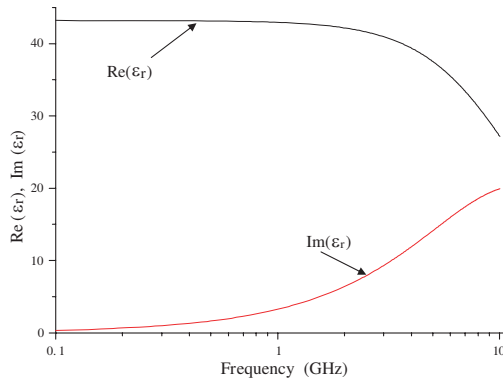


Figure 16. Real and imaginary parts of the permittivity of a lossy host material, where metasheets are embedded.

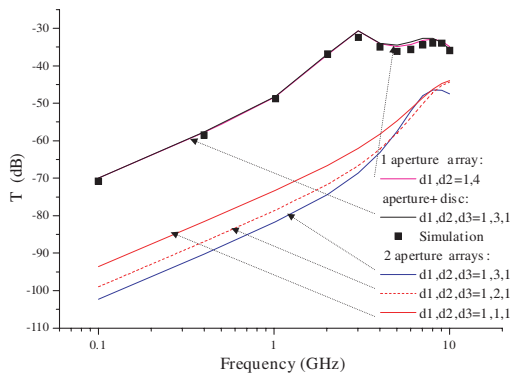


Figure 17. Frequency dependence of transmission coefficient of a two-layered metasheet structure for different separation distances between the metasheets.

5.3.3. Lossy Structure

Consider the same structure as shown in Figure 13. The parameters are the following: the slab is of the thickness $d_1 + d_2 + d_3 = 5$ mm, the cell period is $D_1 = D_2 = 2$ mm, the radius of the aperture is $r_1 = 0.6$ mm, and the radius of the disc is $r_2 = 0.6$ mm. The host dielectric has the Debye frequency response shown in Figure 16. This frequency characteristic is of a composite material that has a Teflon as a host matrix with $\epsilon_r = 2.2$, and carbon inclusions with an aspect ratio of 50, volume fraction 8%, and conductivity $\sigma = 1000$ S/m as a filler. It has been modeled as in [41, 42].

The results of computations based on the presented analytical

model for the normal incidence are shown in Figure 17. In the same figure, the analytical results for a multilayer structure, containing two metasheets, an aperture array and a disk array, are compared with the numerically obtained (HFSS) results. The lowest curve in Figure 17 corresponding to two aperture arrays with distances $d_1 = 1$ mm, $d_2 = 3$ mm, and $d_3 = 1$ mm, is the best solution, providing the lowest transmission coefficient in the frequency range of interest. It was also obtained using an optimization technique based on a genetic algorithm [41]. Varying the dielectric thickness, the location of the MS inside the dielectric slab, the cell periodicity, and the geometry of scatterers, more design freedom can be obtained to synthesize a desirable frequency response of a metasheet structure.

6. CONCLUSION

Analysis and synthesis of frequency characteristics of reflection and transmission coefficients (T and Γ) for single- and multilayered metasheets is critical for the design of frequency-selective structures. Although full-wave numerical methods can provide fairly accurate results, they lose the attraction due to the complexity, large memory consumption, and long computation time. An analytical approach discussed in this paper provides a powerful alternative to numerical computations, since it gives more freedom (variables to be synthesized) for the synthesis, substantially speeds up the synthesis process, and reduces a design cost. With the known (available analytically or numerically beforehand) electric and magnetic polarizabilities of an individual scatter, T and Γ can be directly related to the array period and the geometry parameters of the scatters.

In this paper, the GSTC of a metasheet are reformulated into a concise and simple matrix form, then T and Γ are determined by solving a system of two linear equations for a single-layered patch-type metasheet. T and Γ of the aperture-type metasheet are derived from the complementary structure based on the Babinet's duality principle. The formulas for T and Γ can handle arbitrary incidence angle. For multilayered metasheets, the \mathbf{T} -matrices approach is used to derive T and Γ . The stack is decomposed into 3 types of basic structural elements, and the \mathbf{T} -matrix of the multilayered metasheet is then derived by cascading, i.e., a product of the \mathbf{T} -matrices of all the partial elements. The resultant T and Γ can be readily derived using the overall \mathbf{T} -matrix. Comparison of the analytical results and numerical simulations shows a good agreement, when the array period D is less than 0.5λ (or the more stringent condition is 0.4λ), which also agrees with [21]. The applicable frequency range is expected to be further

extended to higher frequency rang ($D \sim \lambda$), considering interaction between scatters in inhomogeneous local fields, and taking into account higher-order polarizabilities.

Further study will be carried out based on more general case that the metasheet is located in the interface between two different materials. Also, polarizabilities of the other types of scatterers will be studied to enrich the “pattern library” for engineering metamaterial structures.

ACKNOWLEDGMENT

The authors from Missouri University of Science and Technology acknowledge a support in part by a National Science Foundation (NSF), grant No. 0855878 through the I/UCRC program.

APPENDIX A. RELATION BETWEEN T AND Γ FOR COMPLEMENTARY METASHEETS

Consider the metasheet in Figure 4(a) and its complementary structure in Figure 4(b). They are excited by TE and TM incident sources in region I, respectively. They are a pair of dual sources,

$$\vec{E}_2^i = \eta \vec{H}_1^i; \quad \vec{H}_2^i = -\vec{E}_1^i / \eta. \quad (\text{A1})$$

The total fields on the region II of (a) and (b) are [35]:

Region II (a):

$$\begin{aligned} \nabla \times \vec{E}_1 &= -j\omega\mu\vec{H}_1; & \nabla \times \vec{H}_1 &= j\omega\varepsilon\vec{E}_1; \\ \text{boundaryconditions :} & & \begin{cases} \hat{n} \times \vec{E}_1 = 0 & \text{on } \sum \tilde{a} \\ \hat{n} \times \vec{H}_1 = \hat{n} \times \vec{H}_1^i & \text{on } \sum a \end{cases} & (\text{A2}) \end{aligned}$$

Region II (b):

$$\begin{aligned} \nabla \times \vec{E}_2 &= -j\omega\mu\vec{H}_2; & \nabla \times \vec{H}_2 &= j\omega\varepsilon\vec{E}_2; \\ \text{boundaryconditions :} & & \begin{cases} \hat{n} \times \vec{H}_2 = \hat{n} \times \vec{H}_2^i & \text{on } \sum \tilde{a} \\ \hat{n} \times \vec{E}_2 = 0 & \text{on } \sum a \end{cases} & (\text{A3}) \end{aligned}$$

On the other hand, the forward scattered fields in region II $\vec{E}_{1,2}^{s+} = \vec{E}_{1,2} - \vec{E}_{1,2}^i$ and $\vec{H}_{1,2}^{s+} = \vec{H}_{1,2} - \vec{H}_{1,2}^i$ satisfy the following relations:

Region II (a):

$$\begin{aligned} \nabla \times \vec{E}_1^{s+} &= -j\omega\mu\vec{H}_1^{s+}; & \nabla \times \vec{H}_1^{s+} &= j\omega\varepsilon\vec{E}_1^{s+}; \\ \text{boundaryconditions :} & & \begin{cases} \hat{n} \times \vec{E}_1^{s+} = -\hat{n} \times \vec{E}_1^i = \hat{n} \times \eta \vec{H}_2^i & \text{on } \sum \tilde{a} \\ \hat{n} \times \vec{H}_1^{s+} = 0 & \text{on } \sum a \end{cases} & (\text{A4}) \end{aligned}$$

Region II (b):

$$\begin{aligned} \nabla \times \vec{E}_2^{s+} &= -j\omega\mu\vec{H}_2^{s+}; & \nabla \times \vec{H}_2^{s+} &= j\omega\varepsilon\vec{E}_2^{s+}; \\ \text{boundary conditions: } & \begin{cases} \hat{n} \times \vec{H}_2^{s+} = 0 \\ \hat{n} \times \vec{E}_2^{s+} = -\hat{n} \times \vec{E}_2^i = -\hat{n} \times \eta \vec{H}_1^i \end{cases} & \begin{array}{l} \text{on } \sum \tilde{a} \\ \text{on } \sum a \end{array} \end{aligned} \quad (\text{A5})$$

Comparing (A2) and (A5), (A3) and (A4), one can get

$$\begin{aligned} \vec{E}_1^{s+} &= \eta \vec{H}_2; & \vec{E}_2^{s+} &= -\eta \vec{H}_1; \\ \vec{H}_1^{s+} &= -\frac{\vec{E}_2}{\eta}; & \vec{H}_2^{s+} &= \frac{\vec{E}_1}{\eta}. \end{aligned} \quad (\text{A6})$$

The reflected wave is the backward scattered field $\vec{E}_{1,2}^{s-}$ and $\vec{H}_{1,2}^{s-}$ in Region I. The forward and backward scattered fields are related as [36]

$$\begin{aligned} \hat{n} \times \vec{E}^{s-} &= \hat{n} \times \vec{E}^{s+}; & \hat{n} \cdot \vec{E}^{s-} &= -\hat{n} \cdot \vec{E}^{s+}; \\ \hat{n} \times \vec{H}^{s-} &= -\hat{n} \times \vec{H}^{s+}; & \hat{n} \cdot \vec{H}^{s-} &= \hat{n} \cdot \vec{H}^{s+}. \end{aligned} \quad (\text{A7})$$

Then the reflection and transmission coefficients in (a) are

$$\begin{aligned} \Gamma_{TE} &= \frac{E_1^{s-}}{E_1^i} = \frac{E_1^{s+}}{E_1^i} = \frac{\eta H_2}{-\eta H_2^i} = -\tilde{T}_{TM}; \\ T_{TE} &= \frac{E_1}{E_1^i} = \frac{\eta H_2^{s+}}{-\eta H_2^i} = \frac{H_2^{s-}}{H_2^i} = -\tilde{\Gamma}_{TM}. \end{aligned} \quad (\text{A8})$$

Similarly, the following relations can be obtained by exchanging the incident sources in Figures 4(a) and 4(b),

$$\Gamma_{TM} = -\tilde{T}_{TE}; \quad T_{TM} = -\tilde{\Gamma}_{TE} \quad (\text{A9})$$

Additionally, the following relations can be derived from (A7), corresponding to the second equations in (21) and (24), respectively,

$$\begin{cases} \vec{E}_1^t = \vec{E}_1^i + \vec{E}_1^{s+} = \vec{E}_1^i + \vec{E}_1^{s-} = \vec{E}_1^i + \vec{E}_1^r \\ \vec{H}_2^t = \vec{H}_2^i + \vec{H}_2^{s-} = \vec{H}_2^i - \vec{H}_2^{s+} = \vec{H}_2^i - \vec{H}_2^r \end{cases} \Rightarrow \begin{cases} T_{TE} = 1 + \Gamma_{TE} \\ T_{TM} = 1 + \Gamma_{TM} \end{cases} \quad (\text{A10})$$

APPENDIX B. ENERGY CONSERVATION FOR METASHEET MADE FROM PEC

The proof will be carried out based only on a patch-type metasheet. The aperture-type metasheet is dual to the patch-type one, so the energy conservation should fulfill automatically. For definiteness, consider the *TE* case. The *TM* case can be proved by analogy. According to (21),

$$\begin{bmatrix} T_{TE} \\ \Gamma_{TE} \end{bmatrix} = \begin{bmatrix} A_{1,TE} & A_{2,TE} \\ 1 & -1 \end{bmatrix}^{-1} \cdot \begin{bmatrix} A_{3,TE} \\ 1 \end{bmatrix} \quad (\text{B1})$$

Then

$$\begin{aligned}
 |T_{TE}|^2 + |\Gamma_{TE}|^2 &= [T_{TE}^* \ \Gamma_{TE}^*] \cdot \begin{bmatrix} T_{TE} \\ \Gamma_{TE} \end{bmatrix} \\
 &= \left\{ \begin{bmatrix} A_{1,TE} & A_{2,TE} \\ 1 & -1 \end{bmatrix}^{-1} \cdot \begin{bmatrix} A_{3,TE} \\ 1 \end{bmatrix} \right\}^H \begin{bmatrix} A_{1,TE} & A_{2,TE} \\ 1 & -1 \end{bmatrix}^{-1} \cdot \begin{bmatrix} A_{3,TE} \\ 1 \end{bmatrix}, \quad (B2)
 \end{aligned}$$

where “H” means Hermitian operation.

For the PEC case, the coefficients of $A_{1,TE}$, $A_{2,TE}$ and $A_{3,TE}$ in (22) can be expressed according to (43) as

$$\begin{cases} A_{1,TE} = a - jb \\ A_{2,TE} = a - jb \\ A_{3,TE} = a + jb \end{cases}, \quad (B3)$$

where

$$\begin{cases} a = -\frac{\cos \theta}{\eta} \\ b = \frac{1}{2} \omega \alpha_{EE}^{YY} + \frac{k \sin^2 \theta}{2\eta} \alpha_{MM}^{ZZ} \end{cases}. \quad (B4)$$

Then, substituting (B3) and (B4) in (B2), the energy balance is proved,

$$|T_{TE}|^2 + |\Gamma_{TE}|^2 = [a - jb \ 1] \cdot \begin{bmatrix} a + jb & 1 \\ a + jb & -1 \end{bmatrix}^{-1} \cdot \begin{bmatrix} a - jb & a - jb \\ 1 & -1 \end{bmatrix}^{-1} \cdot \begin{bmatrix} a + jb \\ 1 \end{bmatrix} = 1. \quad (B5)$$

REFERENCES

1. Pokrovsky, A. L. and A. L. Efros, “Electrodynamics of metallic photonic crystals and the problem of left-handed materials,” *Phys. Rev. Lett.*, Vol. 89, 093901, 2002.
2. Rahmat-Samii, Y., “The marvels of electromagnetic band gap (EBG) structures: Novel microwave and optical applications,” *Proc. Microwave and Optoelectronics Conference*, 265–275, Sep. 2003.
3. Foteinopoulou, S., E. N. Economou, and C. M. Soukoulis, “Refraction in media with a negative refractive index,” *Phys. Rev. Lett.*, Vol. 90, 107402, 2003.
4. Shvets, G., “Photonic approach to making a material with a negative index of refraction,” *Phys. Rev. B*, Vol. 67, 035109, 2003.
5. Krowne, C. M. and Y. Zhang, *Physics of Negative Refraction and Negative Index Materials, Springer Series in Materials Science*, Vol. 98, Springer, 2007.
6. Wu, T. K., *Frequency Selective Surface and Grid Array*, Wiley, New York, 1995.

7. Munk, B. A., *Frequency Selective Surfaces: Theory and Design*, Wiley, New York, 2000.
8. Munk, B. A., *Metamaterials, Critique and Alternatives*, Wiley, 2007.
9. Knott, E. F., J. F. Shaeffer, and M. T. Tuley, *Radar Cross Section: Its Prediction, Measurement and Reduction*, Ch. 9, Artech House, Dedham, 1986.
10. Narayan, S., K. Prasad, R. U. Nair, and R. M. Jha, "A novel EM analysis of double-layered thick FSS based on MM-GSM technique for radome applications," *Progress In Electromagnetics Research Letters*, Vol. 28, 53–62, 2012.
11. Mahdy, M. R. C., M. R. A. Zuboraj, A. A. N. Ovi, and M. A. Matin, "Novel design of triple band rectangular patch antenna loaded with metamaterial," *Progress In Electromagnetics Research Letters*, Vol. 21, 99–107, 2011.
12. Xu, Z., W. Lin, and L. Kong, "Controllable absorbing structure of metamaterial at microwave," *Progress In Electromagnetics Research*, Vol. 69, 117–125, 2007.
13. Mittra, R., C. H. Chan, and T. Cwik, "Techniques for analyzing frequency selective surfaces—a review," *Proceedings of the IEEE*, Vol. 76, No. 12, 1593–1615, Dec. 1988.
14. Lockyer, D. S., J. C. Vardaxoglou, and R. A. Simpkin, "Complementary frequency selective surfaces," *IEE Proceedings — Microwaves, Antennas and Propagation*, Vol. 147, No. 6, 501–507, Dec. 2000.
15. Moss, C. D., T. M. Grzegorzczuk, Y. Zhang, and J. A. Kong, "Numerical studies of left-handed metamaterials," *Progress In Electromagnetics Research*, Vol. 35, 315–334, 2002.
16. Kuester, E. F., M. A. Mohamed, M. Piket-May, and C. L. Holloway, "Averaged transition conditions for electromagnetic fields at a metafilm," *IEEE Trans. Antennas Propagat.*, Vol. 51, No. 10, 2641–2651, Oct. 2003.
17. Levy-Nathanson, R. and D. J. Bergman, "Decoupling and testing of the generalized Ohm's law," *Phys. Rev. B*, Vol. 55, 5425–5439, 1997.
18. Lee, S. W., G. Zarrillo, and C. L. Law, "Simple formulas for transmission through periodic metal grids or plates," *IEEE Trans. Antennas Propagat.*, Vol. 30, No. 5, 904–909, 1982.
19. Kazantsev, Y. N., V. P. Mal'tsev, and A. D. Shatrov, "Diffraction of a plane wave from a two-dimensional grating of elements with inductive and capacitive coupling," *Journal of Communications*

- Technology and Electronics*, Vol. 46, No. 12, 1303–1313, Dec. 2001.
20. Yatsenko, V. V., S. I. Maslovski, S. A. Tretyakov, S. L. Prosvirnin, and S. Zouhdi, “Plane-wave reflection from double arrays of small magnetoelectric scatterers,” *IEEE Trans. Antennas Propagat.*, Vol. 51, No. 1, 2–11, Jan. 2003.
 21. Holloway, C. L., M. A. Mohamed, and E. F. Kuester, “Reflection and transmission properties of a metafilm with application to a controllable surface composed of resonant particles,” *IEEE Trans. Electromag. Compat.*, Vol. 47, No. 4, 1–13, Oct. 2005.
 22. De Meulenaere, F. and J. Van Bladel, “Polarizability of some small apertures,” *IEEE Trans. Antennas Propagat.*, Vol. 25, No. 2, 198–205, Mar. 1977.
 23. Fabrikant, V. I., “Magnetic polarizability of small apertures: Analytical approach,” *J. Phys. A: Math. Gen.*, Vol. 20, 328–338, 1987.
 24. McDonald, N. A., “Polynomial approximations for the electric polarizabilities of some small apertures,” *IEEE Trans. Microw. Theory Techn.*, Vol. 33, No. 11, 1146–1149, Nov. 1985.
 25. McDonald, N. A., “Polynomial approximations for the transverse magnetic polarizabilities of some small apertures,” *IEEE Trans. Microw. Theory Techn.*, Vol. 35, No. 1, 20–23, Jan. 1987.
 26. Podosenov, S. A., A. A. Sokolov, and S. V. Al’betkov, “Method for determining the electric and magnetic polarizability of arbitrarily shaped conducting bodies,” *IEEE Trans. Electromag. Compat.*, Vol. 39, No. 1, 1–10, Feb. 1997.
 27. Marques, R., F. Mesa, J. Martel, and F. Medina, “Comparative analysis of edge- and broadside-coupled split ring resonators for metamaterial design — Theory and experiments,” *IEEE Trans. Antennas Propagat.*, Vol. 51, No. 10, 2572–2581, Oct. 2003.
 28. Simovski, C. R. and P. A. Belov, “Backward wave region and negative material parameters of a structure formed by lattices of wires and split-ring resonators,” *IEEE Trans. Antennas Propagat.*, Vol. 51, No. 10, 2582–2591, Oct. 2003.
 29. Sauviac, B., “Double split-ring resonators: Analytical modeling and numerical simulations,” *Electromagnetics*, Vol. 24, No. 5, 317–338, 2004.
 30. Simovski, C. R., M. S. Kondratjev, P. A. Belov, and S. A. Tretyakov, “Interaction effects in two-dimensional bianisotropic arrays,” *IEEE Trans. Antennas Propagat.*, Vol. 47, No. 9, 1429–1439, Sept. 1999.
 31. Collin, R. E., *Field Theory of Guided Waves*, 2nd edition, 1991.

32. Maslovski S. I. and S. A. Tretyakov, "Full-wave interaction field in two-dimensional arrays of dipole scatterers," *Int. J. Electron. Commun.*, Vol. 53, 135–139, Arch. Elek. Übertragungstechn. (AEÜ), 1999.
33. Idemen, M., "Straightforward derivation of boundary conditions on sheet simulating an anisotropic thin layer," *Electron. Lett.*, Vol. 24, 663–665, 1988.
34. Idemen, M., "Universal boundary relations of the electromagnetic field," *J. Phys. Soc. Japan.*, Vol. 59, 71–80, 1990.
35. Kong, J. A., *Electromagnetic Wave Theory*, 2nd edition, Wiley, New York, 1990.
36. Jackson, J. D., *Classical Electrodynamics*, 3rd edition, Wiley, New York, 1999.
37. Inan, U. and A. Inan, *Electromagnetic Waves*, Ch. 3.5, Prentice Hall, New Jersey, 2000.
38. Weber, R. J., *Introduction to Microwave Circuits: Radio Frequency and Design Application*, Ch. 2, 25–27, IEEE, New York, 2001.
39. Eggimann, W. H. and R. E. Collin, "Dynamic interaction fields in a two-dimensional lattice," *IEEE Trans. Microw. Theory Techn.*, Vol. 9, No. 2, 110–115, Mar. 1961.
40. Eggimann, W. H., "Higher-order evaluation of electromagnetic diffraction by circular disks," *IEEE Trans. Microw. Theory Techn.*, Vol. 9, No. 5, 408–418, Sep. 1961.
41. Huang, J. Y., P. C. Ravva, M. Y. Koledintseva, R. E. DuBroff, J. L. Drewniak, B. Archambeault, and K. N. Rozanov, "Design of a metafilm-composite dielectric shielding structure using a genetic algorithm," *Progress In Electromagnetics Research Symposium*, 297–301, Cambridge, MA, USA, Mar. 26–29, 2006.
42. Koledintseva, M. Y., J. L. Drewniak, R. E. DuBroff, K. N. Rozanov, and B. Archambeault, "Modeling of shielding composite materials and structures for microwave frequencies," *Progress In Electromagnetic Research B*, Vol. 15, 197–215, 2009.